Journal of Crystal Growth 311 (2009) 4374–4380

Contents lists available at ScienceDirect

Journal of Crystal Growth

journal homepage: www.elsevier.com/locate/jcrysgro

Calculation of phase diagrams in $Al_xIn_{1-x}As/InP$, $As_xSb_{1-x}Al/InP$ and $Al_xIn_{1-x}Sb/InSb$ nano-film systems

Y. Lu, C.P. Wang, X.J. Liu *

Department of Materials Science and Engineering, College of Materials, Research Center of Materials Design and Applications, Xiamen University, Xiamen 361005, PR China

ARTICLE INFO

Article history:
Received 18 December 2008
Received in revised form
11 May 2009
Accepted 27 July 2009
Communicated by G.B. Stringfellow
Available online 5 August 2009

PACS:
81.30.Dz
64.75.St
81.05.Ea

Keywords:
Thin film
Semiconductor
Phase diagram
AlAs–InAs
AlAs–AlSb
AlSb–InSb

ABSTRACT

The models for calculation of phase diagrams of semiconductor thin films with different substrates were proposed by considering the contributions of strain energy, the self-energy of misfit dislocations and surface energy to Gibbs free energy. The phase diagrams of the $Al_xIn_{1-x}As$ and $As_xSb_{1-x}Al$ thin films grown on the InP (1 0 0) substrate, and the $Al_xIn_{1-x}Sb$ thin films grown on the InSb (1 0 0) substrate at various thicknesses were calculated. The calculated results indicate that when the thickness of film is less than 1 μm, the strain-induced zinc-blende phase appears, the region of this phase extends with decreasing of the layer thickness, and there is small effect of surface energies of liquid and solid phases on the phase diagrams.

1. Introduction

The III–V semiconductors are important materials in the fields of fabrication of microwave, optoelectronic, and electronic devices. The film materials of devices are usually obtained by several techniques, such as metal organic vapor phase epitaxy (MOVPE), molecular beam epitaxy (MBE) and liquid phase epitaxy (LPE). Accurate phase diagrams for thin films are very important for understanding of phase transformation in the thin film system, because the growth conditions such as solution composition for the growth and starting growth temperature can be effectively obtained from phase diagram [1,2]. However, the solid compositions of epitaxial film are not precisely consistent with those determined by the equilibrium phase diagram of bulk materials, because the epitaxial films grown on a substrate is affected by the additional energies, such as surface energy, strain energy as well as the energy of misfit dislocations, which are always ignored in bulk materials.

Studies of III–V semiconductors have indicated that these additional energies have considerable influence on phase transformation [3–6]. The III–V ternary compounds can be stabilized and the composition-latching phenomenon appears by the effect of strain in a certain range of solution composition [7,8]. Nakajima et al. [9] calculated the In–Ga–As ternary phase diagram by adding the excess energies to the chemical free energy to explain the extraordinary behavior of the liquid–solid equilibrium near the lattice-matched composition of InGaAs on InP. Ohtani et al. [10] calculated the phase diagrams of some strained III–V semiconductors by considering the strain energy to interpret the composition-latching phenomenon. However, there is no systematic information of liquid–solid equilibrium and the miscibility gap in the whole range of composition for the epitaxial film/substrate structure when the film thickness is thinner than 100 nm.

The purpose of the present work is: (a) to propose a method for calculating the phase diagrams of thin films with different substrates by considering the contributions of strain energy, the self-energy of misfit dislocations and surface energy to Gibbs free energy, and (b) to calculate the pseudobinary section phase diagrams of AlAs–InAs with substrate InP, AlAs–AlSb with substrate InP and AlSb–InSb with substrate InSb.

* Corresponding author. Tel.: +0086 592 2187888; fax: +0086 592 2187966.
E-mail address: lxj@xmu.edu.cn (X.J. Liu).

0022-0248/$ - see front matter © 2009 Elsevier B.V. All rights reserved.
doi:10.1016/j.jcrysgro.2009.07.038

2. Models of Gibbs free energies

In the calculation of Gibbs free energy in the film–substrate system, besides the chemical free energy, the strain energy, self-energy of dislocations and the surface energies of solid and liquid phases should be taken into account, when the film is in nano-scale.

2.1. Chemical Gibbs free energy

The chemical Gibbs free energies of the liquid phase and the zinc-blende phase ξ ((A, B)C) in A–B–C ternary system are respectively described by the regular solution model and two-sublattice model, as follows:

for liquid phase,

$$G^{liq} = {}^0G_A^{liq}x_A + {}^0G_B^{liq}x_B + {}^0G_C^{liq}x_C + RT(x_A\ln x_A + x_B\ln x_B + x_C\ln x_C) + L_{A,B}^{liq}x_Ax_B + L_{A,C}^{liq}x_Ax_C + L_{B,C}^{liq}x_Bx_C + L_{A,B,C}^{liq}x_Ax_Bx_C \quad (1)$$

for zinc-blende phase,

$$G^{\xi} = {}^0G_{A:C}y_A^I + {}^0G_{B:C}y_B^I + RT(y_A^I\ln y_A^I + y_B^I\ln y_B^I) + L_{A,B:C}y_A^Iy_B^I \quad (2)$$

where $L_{i,j}{}^{lig}$ is the i–j interaction parameter in the liquid phase, $L_{A,B:C}$ the A–B interaction in the first sublattice when the second sublattice is occupied by component C. x_A, x_B and x_C are the mole fractions of A, B and C components, ${y_A}^I$ and ${y_B}^I$ are the site fractions of A and B in the first sublattice, respectively.

2.2. Strain energy

The strain energy between the epitaxial layer and substrate was discussed by Ohtani et al. [10]. The strain energy is generated by lattice mismatch, and piles up as the layer thickness increases. Therefore, the strain energy has different expressions below and over the critical thickness, at which the first misfit dislocation has been generated. Contribution of the strain energy to Gibbs free energy is given as follows:

$$G^{st} = \frac{\mu}{2}\frac{1+\upsilon}{1-\upsilon}N_Aa^3f^2 \text{ for } h<h_c \quad (3)$$

$$G^{st} = \frac{N_Aa^3}{4h}\Delta\left(1+\ln\left(\frac{h}{h_c}\right)\right) \text{ for } h\geq h_c \quad (4)$$

where a is the lattice parameter, μ the shear modulus, v the Poisson's ratio, N_A the Avogadro's number, f the misfit between the epitaxial layer and the substrate, and is given by $f=(a-a_0)/a_0$, where a_0 the lattice parameter of the substrate. h and h_c are respectively the layer thickness and critical layer thickness. Δ the energy barrier, and the value of Δ is assumed to be 0.8 (J/m^2) [10,11] for the (1 0 0) orientation.

2.3. Self-energy of misfit dislocations

Because the misfit dislocations exist when epitaxial layer grows over the critical thickness, the contribution of misfit dislocation to the Gibbs free energy should be taken into account. The energy of misfit dislocations of per unit volume is given as follows [12]:

$$G^{dis} = (f-\varepsilon)\frac{b}{\pi(1-\upsilon)}\frac{\mu_0\mu}{\mu_0+\mu}(1-\upsilon\cos^2\alpha)\left[\ln\left(\frac{h}{b}\right)+1\right] \quad (5)$$

where ε is the strain of epitaxial layer over critical thickness, μ_0 the shear modulus of the substrate. α the angle between the dislocation and its Burgers vector $\vec{\boldsymbol{b}}$. The Burgers vectors of the dislocations that generated in III–V semiconductor thin films grown on the (1 0 0) substrate, usually inclined at 60° to the dislocation lines (60° type misfit dislocations), which was observed in Ref. [13]. Thus, the 60° type misfit dislocation is assumed in this paper. In this case, $b=a/\sqrt{2}$, $\alpha=60°$.

2.4. Surface energy

2.4.1. Surface energy of the liquid phase

The liquid surface of a molten solution can be treated as a 'surface phase', the surface tension of the liquid phase can be given using Butler's [14] equations as follows:

$$\sigma = \sigma_i + \frac{RT}{A_i}\ln\frac{a_i^s}{a_i^b} \quad (6)$$

where σ and σ_I are the surface tensions of the molten solution and pure component i, respectively. A_i the molar surface area of the species i, which can be derived from:

$$A_i = 1.091\,N_A^{1/3}V_i^{2/3} \quad (7)$$

where V_i is the mole volume of component i. ${a_i}^s$ and ${a_i}^b$ the activities of component i in bulk and surface phases, respectively. The activities in bulk and surface phases were approximately replaced with the mole fraction in this work. Therefore, the surface energy of the liquid phase of per mole layer contribution to Gibbs free energy can be written by:

$$G_L^{sur} = A_S\sigma \quad (8)$$

where A_S is the surface area of the film.

2.4.2. Surface energy of the solid phase

The surface energy between the vapor and solid phases can be estimated by the bond-cutting theory. The surface energy per unit area of zinc-blende phase can be given approximately by [15]:

$$\gamma_s = (1-w/u)\Delta H_{v0}N_0^{2/3} \quad (9)$$

where u is the number of nearest neighbors of an atom in the bulk of the solid, w the number of neighbors in the solid of an atom on the face. The term $(1-w/u)$ means the number of dangling bonds of an atom on the surface. ΔH_{v0} the enthalpy of evaporation of the material, and N_0 the number of atoms per unit volume. It was assumed that the maximum surface energy before reconstruction of dangling bonds on the surface is the energy to break all of the nearest neighbor bonds across a given plane. The number of atoms per unit surface area (N_S) can be related to the number of atoms per unit volume N_0 as follows:

$$N_S = N_0^{2/3} \quad (10)$$

For the (1 0 0) surface of zinc-blende phase, $N_0^{2/3}$ is given by:

$$N_0^{2/3} = 2/a^2 \quad (11)$$

ΔH_{v0} is given by the enthalpy of evaporation ΔH per mole as follows:

$$\Delta H_{v0} = \frac{\Delta H}{2N_A} \quad (12)$$

The details of expression for ΔH are given in the Appendix A. The molar surface energy depends on the layer thickness, since the total volume per mole is constant. Thus, the surface energy of per mole layer contribution to Gibbs free energy can be written as

follows:

$$G_S^{sur} = \alpha A_S \gamma_S \quad (13)$$

where α is the reconstruction parameter on the surface, which means the ratio of the surface energy between after reconstruction and before reconstruction of dangling bonds on the surface. The values of α used in this paper are listed in Table 1 [16–18].

2.5. Total energy of the film

Total Gibbs free energy of the liquid and zinc-blende phases were given by the sum of the chemical energy and the additional free energies as follows:

for liquid phase,

$$G^{film} = G^{liq} + G_L^{sur} \quad (14)$$

for zinc-blende phase,

$$G^{film} = G^{\xi} + G^{st} + G_S^{sur} \text{ for } h < h_c \quad (15)$$

$$G^{film} = G^{\xi} + G^{st} + G_S^{sur} + G^{dis} \text{ for } h \geq h_c \quad (16)$$

On the basis of Eqs. (14)–(16), the phase diagrams of the AlAs–InAs, AlAs–AlSb and AlSb–InSb pseudobinary section with different film thicknesses can be calculated.

3. Calculated results

3.1. Evaluation of parameter

The thermodynamic parameters of the Al–In–As, As–Al–Sb and Al–In–Sb systems [19,20] are listed in Table 2, the elastic parameters and some required parameters of pure elements used in the calculation are respectively listed in Table 3 [9,21] and Table 4 [22]. The value of surface tension of pure arsenic is assumed to be zero, because of no experimental information. The thermodynamic data used to calculate ΔH were obtained from Ref. [23].

Table 1
Surface reconstruction and reconstruction parameter (α) for ternary alloys [16–18].

Alloy	Surface reconstruction (1 0 0)	N_d^r	N_d^b	N_d^r/N_d^b (α)[a]
$Al_xIn_{1-x}As$	(2×3) [16]	$4/3a^2$	$4/a^2$	0.333
$As_xSb_{1-x}Al$	(1×3) [17]	$2/a^2$		0.500
$Al_xIn_{1-x}Sb$	(1×3) [18]	$2/a^2$		0.500

[a] N_d^b and N_d^r are the numbers of dangling bonds of surface before and after reconstruction, respectively.

3.2. The excess free energies of $Al_xIn_{1-x}As$ film grown on InP substrate

The surface energy, strain energy and self-energy of dislocations of $Al_xIn_{1-x}As$ layer grown on the InP substrate were calculated. Fig. 1(a) shows the calculated strain energy of the $Al_xIn_{1-x}As$ film at various thicknesses. The strain energy below critical film thickness (the dash line) and the sum of the strain energy and the self-energy of dislocations over critical thickness (the solid line) at different film thicknesses were calculated. It can be seen that the energies increase as the film thickness increases over h_c. Fig. 1(b) illustrates the lattice constants of the substrate and films as a function of the composition of the component AlAs, where the lattice-matched composition (LMC) between $Al_xIn_{1-x}As$ layer and the substrate InP is 47.7%. This means that the values of strain energies at the LMC disappear, and increase as the AlAs composition increases or decreases from $x_{AlAs} = 47.7\%$, due to the stress relief and the dislocation generation. Fig. 2 shows the solid–gas surface energies of solid film, where the surface energies increase as the AlAs compositions increase. Fig. 3 shows the curves of different energies calculated by considering the chemical energy, surface energies, strain energy and self-energy of dislocations, where the dash line is the chemical Gibbs free energy curve of the system, the dashdotted line indicates the contributions of strain energy and self-energy of dislocations and the solid line is the total energy including strain energy, self-energy of dislocations, surface energy and chemical Gibbs free energy. It is seen that the strain energy heighten the energy curve on both sides of the LMC, while, the surface energy raises the whole energy curve.

3.3. Phase diagrams of $Al_xIn_{1-x}As$/InP film at various thicknesses

Fig. 4 shows the calculated phase equilibria of the $Al_xIn_{1-x}As$ epitaxial film grown on the (1 0 0)-oriented InP at various thicknesses. The dash lines are the pseudobinary phase diagram of bulk $Al_xIn_{1-x}As$, and a spinodal decomposition appears at lower temperature. The calculated results indicate that there are three characteristics for the phase diagram of $Al_xIn_{1-x}As$ film: (1) three phases of AlAs, InAs and ξ' appear at lower temperature and all of

Table 3
Elastic parameters for binary compound [9,21].

	Lattice parameter a (nm)	shear modulus $\mu(\times10^{10}(N/m^2))$ (1 0 0)	Poisson's ratio ν(1 0 0)
AlAs	0.5661	2.945	0.32
InAs	0.6058	1.980	0.35
InP	0.5869	2.280	0.36
AlSb	0.6136	2.488	0.31
InSb	0.6479	1.510	0.34

Table 2
Thermodynamic parameters for ternary alloys [19,20].

System	Phase	Thermodynamic parameters ($J\,mol^{-1}$)	Ref.
Al–As–In	Liquid phase	$L^{liq}_{Al,As,In} = -74112.5$	[19]
	Zinc-blende compound (ξ)	$L^{\xi}_{Al,In:As} = 6250$	[19]
Al–As–Sb	Liquid phase	$L^{liq}_{Al,As,Sb} = 0$	[20]
	Zinc-blende compound (ξ)	$L^{\xi}_{As,Sb:,Al} = 17560$	[20]
Al–In–Sb	Liquid phase	$L^{liq}_{Al,In,Sb} = -7450y_{Al}-39116y_{In}-30296y_{Sb}$	[20]
	Zinc-blende compound (ξ)	$L^{\xi}_{Al,In:Sb} = 1105$	[19]

Table 4
Mole volume and surface tension data for pure elements [22].

V_{Al} (m^3/mol) = 26.98/(2.385 × 10^6−280 × (T-933.15))
V_{As} (m^3/mol) = 74.9216/(5.22 × 10^6−535 × (T-1090.2))
V_{In} (m^3/mol) = 114.818/(7.032 × 10^6−679.8 × (T-429.75))
V_{Sb} (m^3/mol) = 121.76/(6.483 × 10^6−565 × (T-903.65))
σ_{Al} (N/m) = 0.914–0.00035 × (T-933.15)
σ_{In} (N/m) = 0.556–0.00009 × (T-429.75)
σ_{Sb} (N/m) = 0.367–0.00005 × (T-903.65)

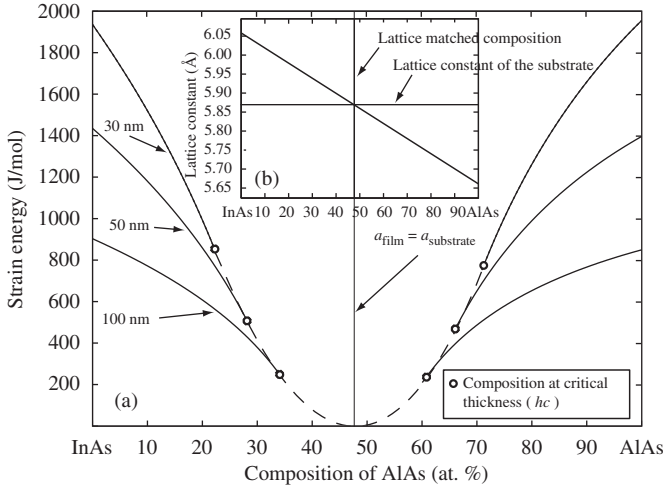

Fig. 1. Calculated strain energy of the $Al_xIn_{1-x}As$ film at various thicknesses (a), and the lattice constant of the $Al_xIn_{1-x}As$ film as a function of the composition of the component AlAs (b).

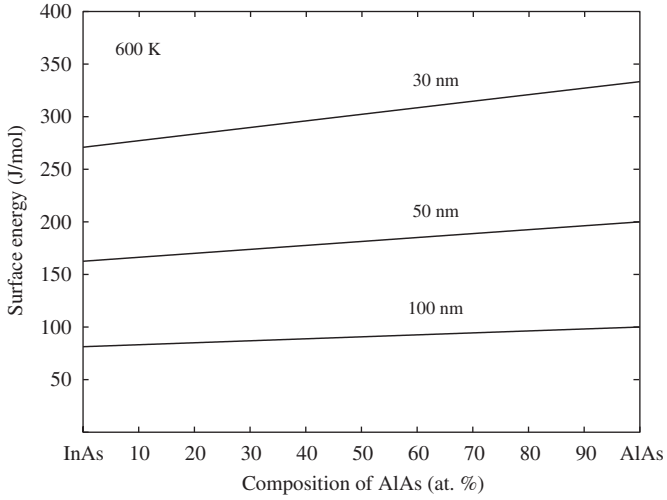

Fig. 2. Calculated surface energy of $Al_xIn_{1-x}As$/InP film at various thicknesses.

them have the same crystal structure. AlAs and InAs are the AlAs-rich and InAs-rich solid solution. ξ′ is a new strain-induced zinc-blende phase. (2) The liquidus of the film is lower than that of the bulk materials, but the solidus of the film is lower or higher than that of the bulk materials at the left and right sides of the LMC (47.7%), respectively. (3) There exist two peritectic reactions of the AlAs+liquid→ξ′ and ξ′+liquid→InAs in the $Al_xIn_{1-x}As$ phase

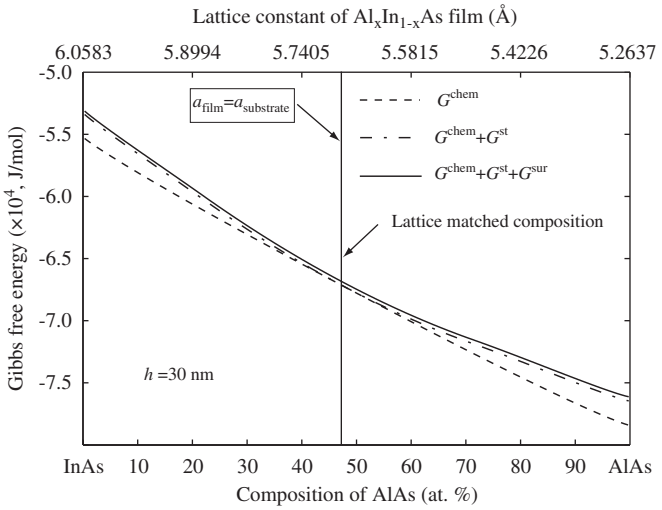

Fig. 3. Gibbs free energy of $Al_xIn_{1-x}As$/InP film calculated by different methods at 600 K.

diagrams, and temperatures of these peritectic reactions increase as the film thickness decreases.

3.4. Phase diagrams of $As_xSb_{1-x}Al$/InP and $Al_xIn_{1-x}Sb$/InSb films

Fig. 5 shows the calculated phase diagrams of the $As_xSb_{1-x}Al$/InP film with different thicknesses of 30, 50 and 100 nm, where the dash lines are the pseudobinary phase diagram of bulk $As_xSb_{1-x}Al$. The changes of liquidus and solidus have the same characteristics with those of the $Al_xIn_{1-x}As$/InP film, and the LMC is 56.27%. The calculated results indicate that AlSb-rich (marked by AlSb), InSb-rich (marked by InSb) solid solution and ξ′ phase also appear at lower temperature. Two peritectic reactions of the AlAs+liquid→ξ′ and ξ′+liquid→AlSb exist in the $Al_xIn_{1-x}As$/InP film phase diagrams. The ξ′ phase region enlarges as the film thickness decreases. The calculated phase diagrams of $Al_xIn_{1-x}Sb$/InSb film with thicknesses of 30 and 50 nm are shown in Fig. 6, where the dash lines are the pseudobinary phase diagram of bulk $Al_xIn_{1-x}Sb$. The temperatures of liquidus and solidus of the film are lower than that of the bulk materials, and the peritectic reactions of the AlSb+liquid→InSb appears.

4. Discussion

We systemically studied the various defects that may exist in preparing films and their contributions in total energy of the system. The strain energy increases as the strained film grows thicker. When the strain energy is large enough, the misfit dislocations generate at the interface between the film and the substrate. However, the strained film only appears in the compositional range as shown by the dash line in Fig. 1, where the strain-induced zinc-blende (ξ′) phase appears in the calculated phase diagrams, because there are two strain-induced spinodal decompositions on both sides of the LMC due to the strain energy in this compositional range (for $Al_xIn_{1-x}Sb$/InSb system, there is one strain-induced spinodal decomposition). While in the compositional ranges as shown by the solid lines in Fig. 1, the film becomes relaxed because of the appearance of misfit dislocation.

Table 5 lists the calculated results of the temperatures and equilibrium compositions of peritectic reactions in the film/substrate system. It is seen that both of the temperatures and equilibrium compositions of peritectic reactions of the AlAs+liquid→ξ′ and AlSb+liquid→InSb increase as the film thicknesses decrease.

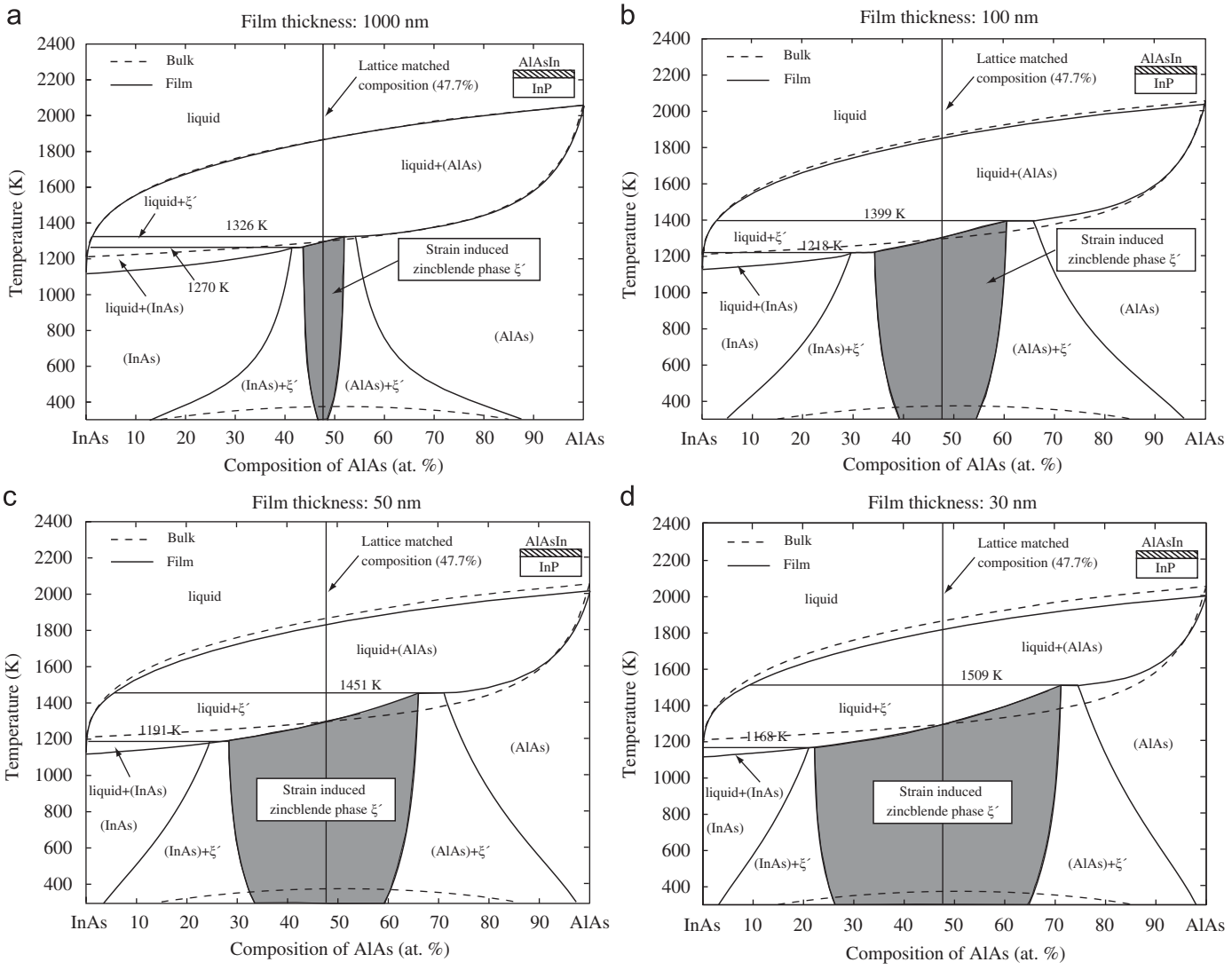

Fig. 4. Calculated phase diagram of $Al_xIn_{1-x}As$/InP film at thicknesses of (a) 1000 nm, (b) 100 nm, (c) 50 nm and (d) 30 nm.

While these of the peritectic reactions of the ξ′+liquid→InAs and ξ′+liquid→AlSb decrease with the film thicknesses.

In this calculation, we also considered the effect of surface energy after surface reconstruction on the phase diagram in the film system. Fig. 7 shows the effect of surface energy of the zinc-blende phase on phase equilibria, where the dash and solid lines indicate the Gibbs free energies without and with the contribution of surface energy, respectively. The equilibrium compositions of the strain-induced zinc-blende phase as shown by dash line are almost the same with that as shown by solid line. Although the surface energy heightens the Gibbs free energy curve in the entire compositional range (Fig. 3), there is no change in the shape of the Gibbs free energy curve. Accordingly, the surface energy can increases the total energy of the system, but has small effect on the phase equilibria.

5. Conclusions

The model of phase diagram calculation of thin film was proposed by considering the contributions of strain energy, self-energy of dislocations and surface energy to Gibbs free energy, and the phase diagrams of the $Al_xIn_{1-x}As$/InP, $As_xSb_{1-x}Al$/InP and $Al_xIn_{1-x}Sb$/InSb nano-film systems were calculated. It is found that a new strain-induced zinc-blende phase appears and the phase diagrams in nano-film system are largely different from that in bulk systems.

Acknowledgements

This work was supported by the National Natural Science Foundation of China (Nos. 50425101 and 50571084), and the Ministry of Science and Technology (No. 2009DFA52170).

Appendix A. Calculation methods of the expression ΔH

The enthalpy change (ΔH) of one mole of solid $A_xB_{1-x}C$ transferring to the ternary A–B–C vapor at temperature T can be given by

$$\Delta H = H^g_{ABC} - H^S_{ABC} \quad (A.1)$$

where H^g_{ABC} and H^S_{ABC} are the enthalpies of vapor and solid phase, respectively. H^g_{ABC} can be obtained from the summation of enthalpy of the pure A, B and C gases at equilibrium temperature

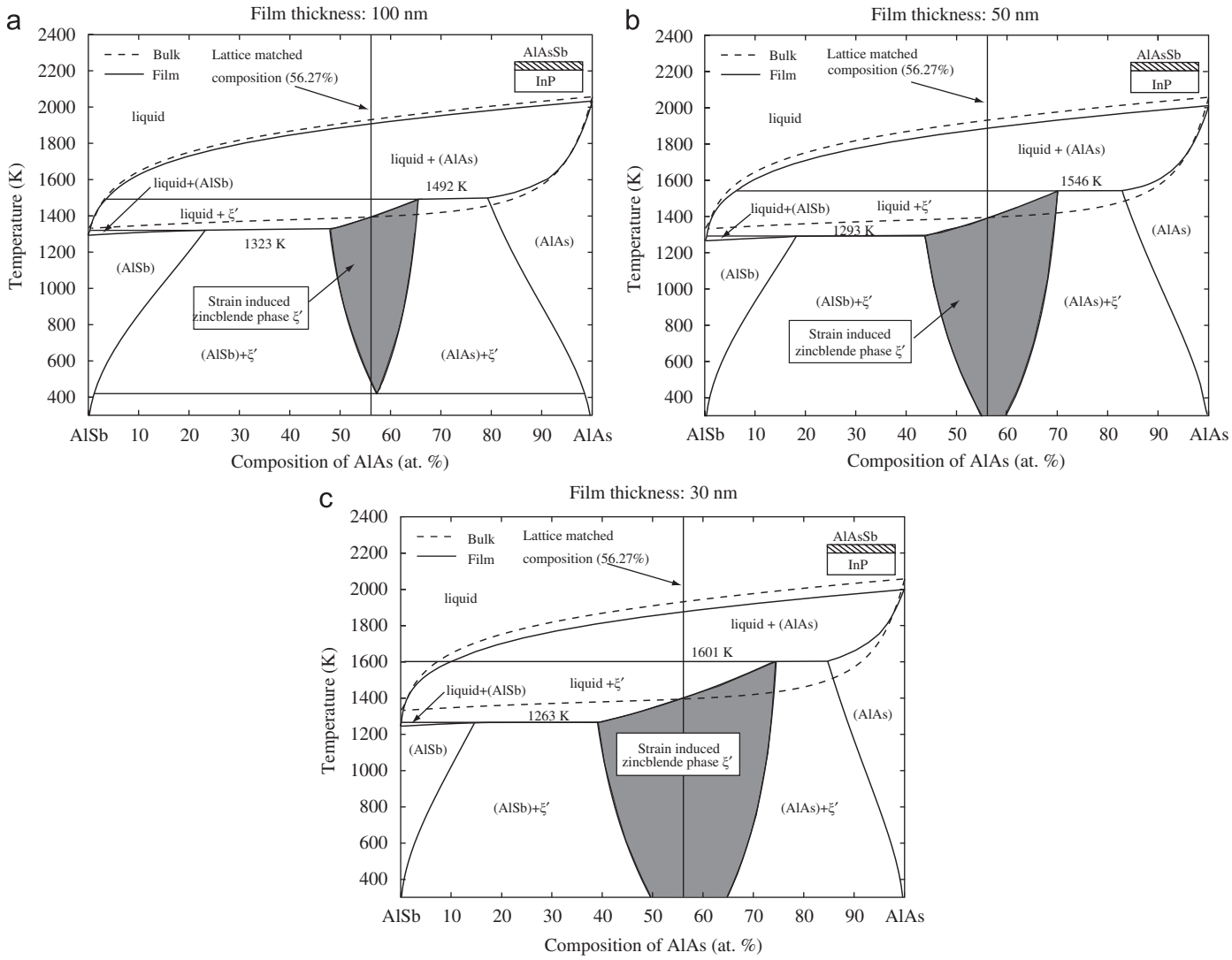

Fig. 5. Calculated phase diagram of $As_xSb_{1-x}Al/InP$ film at thicknesses of (a) 100 nm, (b) 50 nm and (c) 30 nm.

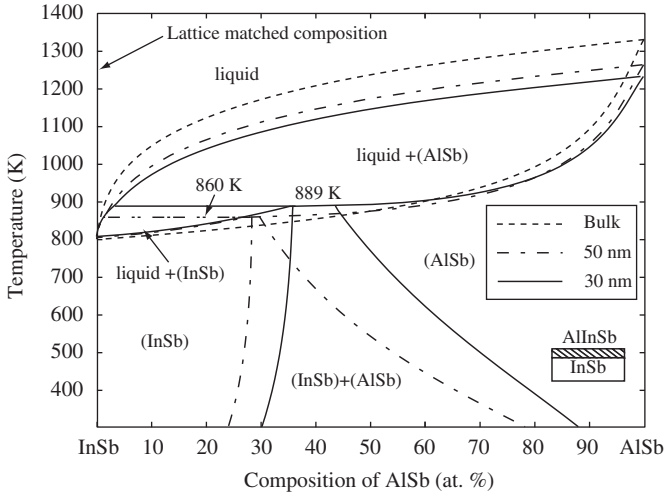

Fig. 6. Calculated phase diagram of $Al_xIn_{1-x}Sb/InSb$ film at thicknesses of 50 and 30 nm.

T, and is given by:

$$H^g_{ABC} = x\left(H^{g,298\,K}_A + \int_{298\,K}^{T} C^A_p(T)\,dT\right) + (0.5-x)\left(H^{g,298\,K}_B + \int_{298\,K}^{T} C^B_p(T)\,dT\right) + 0.5\left(H^{g,298\,K}_C + \int_{298\,K}^{T} C^C_p(T)\,dT\right) \quad (A.2)$$

H^S_{ABC} is given by:

$$H^S_{ABC} = xH^s_{AC} + (1-x)H^s_{BC} + \Delta H^s_{mix(ABC)} \quad (A.3)$$

where H^s_{AC} and H^s_{BC} are the enthalpy of the binary A–C and B–C compound, respectively. H^s_{AC} and H^s_{BC} are given by:

$$H^s_{ABC} = xH^{s,298\,K}_{AC} + x\int_{298\,K}^{T} C^{AC}_p(t)\,dT + (1-x)H^{s,298\,K}_{BC} + (1-x)\int_{298\,K}^{T} C^{BC}_p(T)\,dT \quad (A.4)$$

Table 5
Calculated results of peritectic reactions in the film/substrate system.

Film/substrate system	Peritectic reactions	Phase equilibria	Thickness (nm)	Temperature (K)	Equilibria composition (at%)		
		Phase I/phase II/phase III			Phase I (%)	Phase II (%)	Phase III (%)
$Al_xIn_{1-x}As$/InP	AlAs+liquid→ξ′	Liquid/ξ′/AlAs	1000	1326	1.2	51.8	54.1
			100	1399	3.1	60.6	65.8
			50	1451	5.5	65.9	70.9
			30	1509	9.2	71.1	74.6
	ξ′+liquid→InAs	Liquid/InAs/ξ′	1000	1270	0.5	41.3	43.6
			100	1218	0.2	29.7	34.2
			50	1191	0.1	24.7	28.3
			30	1168	0.05	21.2	22.2
$As_xSb_{1-x}Al$/InP	AlAs+liquid→ξ′	Liquid/ξ′/AlAs	100	1492	3.6	65.5	79.4
			50	1546	6.2	70.0	82.8
			30	1601	10.1	74.6	84.9
	ξ′+liquid→AlSb	Liquid/AlSb/ξ′	100	1323	0.5	23.3	47.9
			50	1293	0.3	18.1	43.8
			30	1263	0.2	14.7	39.2
$Al_xIn_{1-x}Sb$/InSb	AlSb+liquid→InSb	Liquid/InSb/AlSb	50	860	1.5	28.4	29.7
			30	889	3.3	35.9	43.5

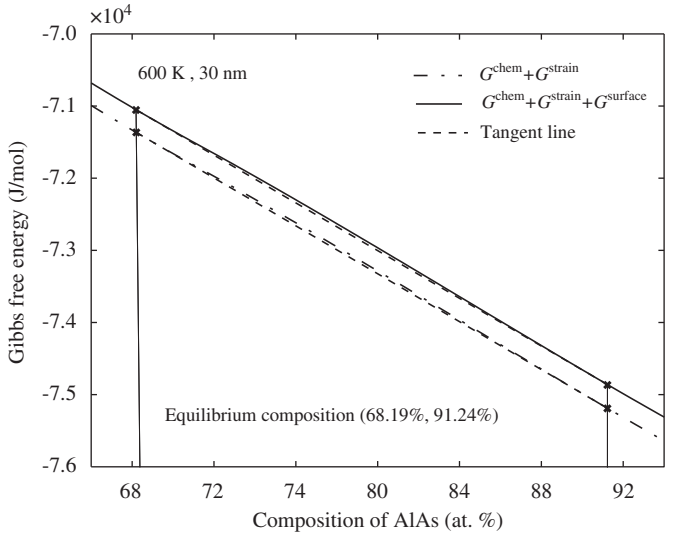

Fig. 7. Phase equilibria of $Al_xIn_{1-x}As$/InP film calculated by two descriptive methods of Gibbs free energy.

the enthalpies of mixing $\Delta H^s_{mix(ABC)}$ can be written using simple solution model as follows:

$$\Delta H^s_{mix(ABC)} = x(1-x)\Omega^s_{AC-BC} \tag{A.5}$$

where Ω^s_{AC-BC} is the interaction parameter of the ternary alloy $A_xB_{1-x}C$. ΔH can be given using Eqs. (A.1)–(A.5) as follows:

$$\begin{aligned}\Delta H = {} & xH_A^{g,298\ K} + (0.5-x)H_B^{g,298\ K} + 0.5H_C^{g,298\ K} \\ & + \int_{298\ K}^{T}\left(xC_p^A + (0.5-x)C_p^B + 0.5C_p^C(T)\right)\mathrm{d}T \\ & -(xH_{AC}^{s,298\ K} + (1-x)H_{BC}^{s,298\ K} \\ & + \int_{298\ K}^{T}(xC_p^{AC} + (1-x)C_p^{BC})(T)dT + x(1-x)\Omega^s_{AC-BC}\Big)\end{aligned}$$

References

[1] P. Capper, M. Mauk, Liquid phase epitaxy of electronic optical and optoelectronic materials, Wiley Series in Materials for Electronic and Optoelectronic Application, England, 2007, pp. 45–83.
[2] G. Müller, Jean-Jacques Métois, P. Rudolph, Crystal Growth: From Fundamentals to Technology, Elsevier, Amsterdam, 2004, pp. 1–21.
[3] C. Lin, A.Z. Li, J. Cryst. Growth 203 (1999) 511.
[4] J.Y. Shen, C. Chatillon, I. Ansara, Calphad 22 (1998) 495.
[5] K. Nakajima, T. Tanahashi, K. Akita, T. Yamaoka, J. Appl. Phys. 50 (1979) 4975.
[6] K. Nakajima, J. Okazaki, J. Electrochem. Soc. 132 (1985) 1424.
[7] B. de Cremoux, J. Phys. Colloq. (Orsay, Fr.) 43 (1982) C5–C19.
[8] G.B. Stringfellow, J. Appl. Phys. 43 (1972) 3455.
[9] K. Nakajima, T. Ujihara, G. Sazaki, N. Usami, J. Cryst. Growth 220 (2000) 413.
[10] H. Ohtani, K. Kobayashi, K. Ishida, J. Phase Equilibria 22 (2001) 276.
[11] T. Yokogawa, H. Sato, M. Ogura, Appl. Phys. Lett. 52 (1988) 3618.
[12] J.W. Matthews, A.E. Blakeslee, J. Cryst. Growth 27 (1974) 118.
[13] P.L. Gourley, I.J. Fritz, L.R. Dawson, Appl. Phys. Lett. 52 (1988) 377.
[14] J.A.V. Butler, Proc. R. Soc. A 135 (1932) 348.
[15] K. Nakajima, Jpn. J. Appl. Phys. 38 (1999) 1875.
[16] A. Gomyo, K. Makita, I. Hino, T. Suzuki, Phys. Rev. Lett. 72 (1994) 673.
[17] S. Németh, B. Grietens, G. Borghs, J. Appl. Phys. 77 (1995) 3552.
[18] W.K. Liu, K.J. Goldammer, M.B. Santos, J. Appl. Phys. 84 (1998) 205.
[19] J.B. Li, W.J. Zhang, C.R. Li, Z.M. Du, Rare Metals 19 (2000) 210.
[20] K. Ishida, H. Tokunaga, H. Ohtani, T. Nishizawa, J. Cryst. Growth 98 (1989) 140.
[21] K. -N. Tu, J.W. Mayer, L.C. Feldman, Electronic Thin Film Sciences, Macmillan College Publishing Company, New York, 1992, p. 464.
[22] Eric A. Brandes, Smithells Metals Reference Book, Butterworth, London, 1983.
[23] Ihsan Barin, Thermochemical Data of Pure Substances, Science publishing company, Beijing, 2003 (in Chinese).